Engineering equifrequency contours of metasurfaces for self-collimated surface-wave steering

Sara M. Kandil,[1,*] Dia'aaldin J. Bisharat,[2] and Daniel F. Sievenpiper[1]

[1] *University of California San Diego, Department of Electrical and Computer Engineering, La Jolla, California 92093, USA*

[2] *City University of New York, Graduate Center, New York, New York 10016, USA*

(Received 5 January 2024; accepted 15 March 2024; published 2 April 2024)

Metasurfaces provide unique capability in guiding surface waves and controlling their polarization and dispersion properties. One way to study their guiding properties is by analyzing their equifrequency contours. Equifrequency contours are the 2D projections of the 3D dispersion diagram. Since they are **k**-space-map representations of the surface, many of the wave properties can be understood from the equifrequency contours. In this paper, we investigate numerically and experimentally the engineering of equifrequency contours using a C-shaped metasurface design. We show the ability to provide high self-collimation as well as spin-dependent wave splitting for the same metasurface by tuning the frequency of operation. We also show the ability to steer the wave along a defined curved path by rotating the C-shaped unit cells, which results in rotation of its equifrequency contours. This work demonstrates how engineering equifrequency contours can be used as a powerful tool for controlling the surface wave propagation properties.

DOI: 10.1103/PhysRevApplied.21.044006

I. INTRODUCTION

During the last decade, there has been great interest in making conventional optics such as lenses, waveguides, couplers, and polarization-based devices using flat surfaces [1–3]. These surface platforms provide the advantage of being scalable and easily integrated on chips. Besides, they provide additional degrees of freedom for controlling the wave propagation as well as eliminating the accumulated changes in phase and amplitude due to propagation over long distances as in the case of conventional optical systems [4].

Metasurfaces, which are 2D surfaces patterned with subwavelength scatterers, are extensively studied as platforms for flat optics. They provide unique capabilities in controlling the dispersion properties, phase, and polarization of the propagating wave [5,6]. This can be done by careful choice of the unit-cell design to engineer the interaction between the wave and the surface. Several studies have investigated the wide capabilities of metasurfaces, including guiding [7–9], focusing [10,11], splitting [12–14], steering [15], and lensing [16]. One way to control the interaction between the wave and the surface is by engineering the equifrequency contour of the unit-cell design. An equifrequency contour (EFC), also called an "isofrequency contour (IFC)," is the 2D projection of the 3D dispersion diagram at different frequencies [17,18]. It represents a **k**-space map of the possible trajectories of the wave at different frequencies. The direction of the wave is determined by the direction of its group velocity, where the group velocity of the wave is defined as $\delta\omega/\delta k$. This can be determined through the EFCs. Anisotropic shapes where some symmetries are broken have interesting, nonconventional EFCs, where the contours can vary from elliptical to flat, allowing the wave to propagate in one direction (normal to the flat contour) with high self-collimation [19].

Another capability of metasurfaces is that they can control the spin-orbit coupling of surface waves. It was recently shown that surface waves with evanescent tails possess a transverse spin that is locked to the wave momentum, a property termed the "spin Hall effect" (SHE) where opposite spins propagate in opposite directions [20–22]. This is analogous to the SHE phenomenon initially discovered in electronic systems [23]. It is also referred to as "spin-momentum locking," where spin represents the circular polarization of the electric and/or magnetic field of the surface wave. It is defined as the right-hand triplet, which is formed of spin, the propagation constant, and the decay constant. It results in spin-dependent propagation of surface waves. Several studies showed the ability to achieve spin-dependent unidirectional propagation using metasurfaces with engineered anisotropy [24–26], bandgap materials [27,28], gradient metasurfaces [29], and near-field interference with asymmetrically placed dipole sources [30–32].

*Corresponding author. skandil@stanford.edu

In this paper, we investigate the different ways the EFC of a metasurface can be engineered to control surface-wave propagation and spin-dependent directionality. We show various wave properties achieved through the same metasurface design, such as self-collimation, polarization-based beam splitting, and wave steering. This paper is organized as follows: In Sec. II, we discuss the homogeneous metasurface design formed of metallic C-shaped unit cells, its self-collimation, and its spin-dependent wave propagation. In Sec. III, we present the inhomogeneous design formed of the same metallic C-shaped unit cells. We discuss how its EFCs change with the rotation angle, resulting in surface-wave steering along two predefined paths. We study these phenomena using numerical simulations as well as experimental results, where the latter are presented in Sec. IV. The paper is concluded in Sec. V.

II. HOMOGENEOUS (PERIODIC) METASURFACE

Figure 1 presents a schematic showing the C-shaped metasurface we study throughout this section. As depicted in Fig. 1(b), the unit cell consists of a metallic C-shaped post of 0.143-mm thickness, placed on top of a Rogers 5880 substrate ($\epsilon_r = 2.2$). The C-shaped metallic post has a width of 0.715 mm and a radius of 2.145 mm, where its edge is extended from the center by 0.429 mm. The whole metasurface is of size 250×250 mm^2, consisting of a 2D array of C-shaped unit cells with periodicity of 5 mm. The C-shaped metasurface was studied and optimized numerically with Ansys HFSS. In this section, we explore different surface-wave properties supported by the C-shaped metasurface by studying its equifrequency contours.

A. Self-collimation

As the asymmetry of the shape increases, the contour becomes flatter with greater wave directionality and, hence, higher self-collimation [33]. The C-shaped design has broken rotational symmetry along the z and x axes, which makes it a low-symmetry shape and allows high self-collimation. This can be observed from the calculated EFC of the C-shaped unit cell shown in Fig. 2(a). The EFCs are calculated by eigenmode simulations for the C-shaped unit cell with use of Ansys HFSS. It can be shown that the C-shaped design possesses different contour shapes, which dictate various wave-propagation properties. At 14 GHz, the EFC is elliptical, and then becomes flatter at higher frequencies, where high self-collimation occurs. More information on the V-shaped electric field propagation for the 14-GHz contour is provided in Sec. S1 in Supplemental Material [34]. The electric field profiles at different frequency contours are shown in Fig. 2(b), where the surface is excited with an E_y dipole at the bottom center of the surface. The magnitude of E_x maps are calculated for each EFC. It can be observed that the wave is split, where the split angle decreases with the increase of frequency. At 19 GHz, the surface wave is highly collimated as well as spin independent. This means that any polarization will excite the wave to propagate with high collimation and zero split angle.

B. Spin-dependent propagation

Figure 2(c) shows the spin-dependent behavior of the supported surface wave. The EFC calculated for the C shape shows a spin-based wave-splitting property, where the wave is split into left-handed and right-handed circularly polarized waves. Through excitation of the surface with an $E_y + iE_z$ dipole source, the wave propagates along the left arm, whereas it propagates along the right arm when excited with an $E_y - iE_z$ dipole source. The spin density is defined as a vector quantity whose direction is normal to the plane of the field circular rotation. The following equation can be used to calculate the spin density of the propagating surface wave [35]:

$$\mathbf{S} = \mathrm{Im}\left\{\frac{\mathbf{E}^* \times \mathbf{E} + \mathbf{H}^* \times \mathbf{H}}{|\mathbf{E}|^2 + |\mathbf{H}|^2}\right\}, \quad (1)$$

where $\mathbf{S}$ is the spin density vector in Gaussian units normalized per photon in the unit of $\hbar = 1$, and $\mathbf{E}$ and $\mathbf{H}$ are the electric and magnetic fields of the surface wave. To better explain the spin-dependent wave-splitting property of the C-shaped metasurface, we study the 16-GHz EFC in Fig. 3 using the spin density function. Figure 3(a)

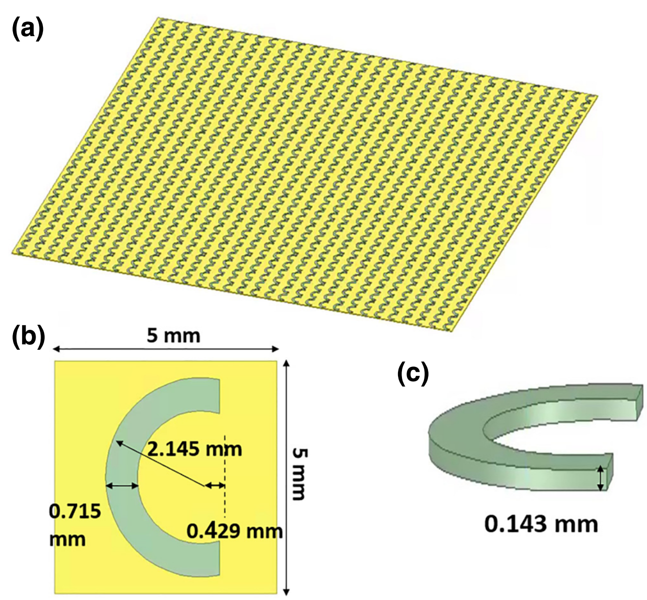

FIG. 1. (a) C-shaped metasurface. (b) Dimensions of the C-shaped unit cell consisting of (c) a C-shaped metallic post of 0.143-mm thickness placed on a Rogers 5880 substrate.

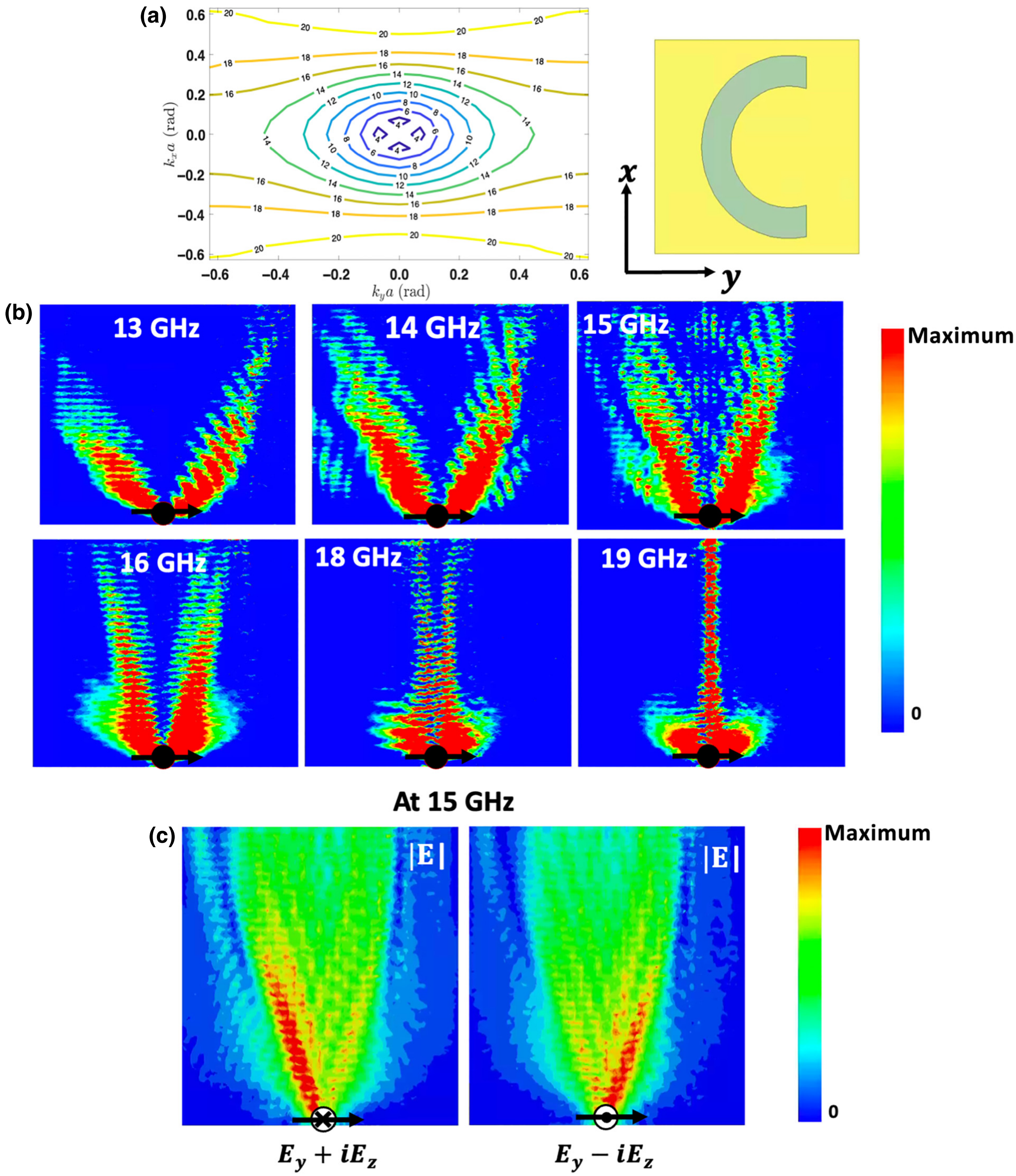

FIG. 2. (a) The C-shape unit cell (right) and its EFC (left). (b) Magnitude of E_x profiles for the C-shaped metasurface calculated at frequencies from 13 to 19 GHz when excited with an E_y dipole source at the bottom center. (c) Magnitude of E_x profiles for the C-shaped metasurface calculated at 15 GHz when excited at the bottom center with $E_y + iE_z$ (left) and $E_y - iE_z$ (right).

shows the 16-GHz EFC of the C-shaped metasurface and a schematic representation of the two wave-propagation directions (k along the left and right directions) with the transverse spin, S, normal to the k direction due to the spin-momentum locking of surface waves. The two components of the transverse spin (S_x and S_y) are shown with respect to the two wave-propagation directions. It can be observed that the S_x component flips sign, while the

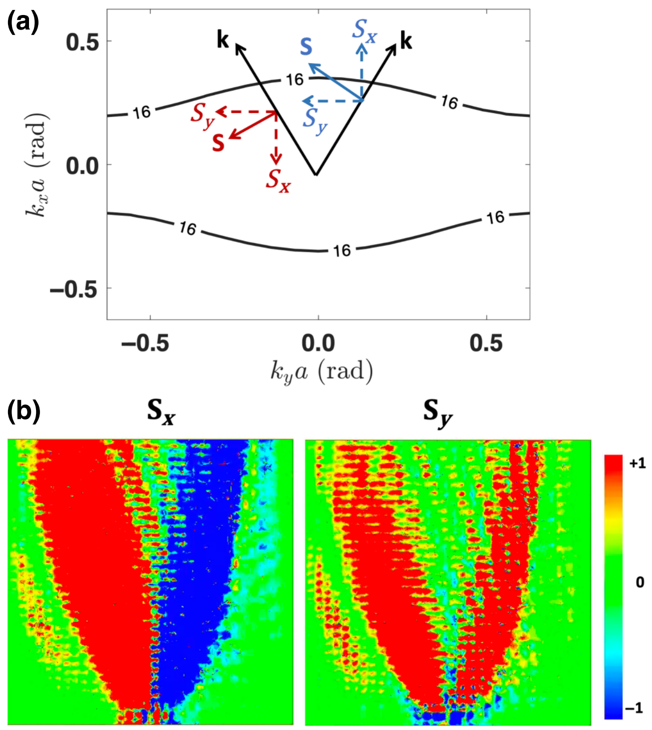

FIG. 3. (a) The 16-GHz EFC of the C-shaped unit cell, where the **k**-vector directions and transverse spin components are depicted. (b) The x component (left) and y-component (right) of the transverse spin density vector calculated for the surface wave supported by the C-shaped metasurface at 16 GHz.

S_y component maintains the same sign for both k directions. This is verified in Fig. 3(b), which presents the numerically calculated normalized spin values for the two split waves for the two transverse spins, S_x and S_y. As shown, S_y is positive along the two directions, while S_x has opposite signs (where $+1$ is represented by red and -1 is represented by blue). S_x is produced by the circularly polarized dipole source: $E_y \pm iE_z$.

III. INHOMOGENEOUS (GRADED) METASURFACE

As demonstrated, the EFC is closely related to the shape of the unit cell; it can be engineered in different ways. For example, some studies showed that the change of the unit cell from square to rectangular or a parallelogram can increase the flatness of the EFCs and hence increase the collimation [36,37]. The symmetry of the shape itself can also result in a change in the contour shape. For example, as described earlier, a broken rotational symmetry can produce flatter contours along the x axis or the y axis. Forty-five-degree mirror symmetry of a shape can result in tilted contours [38].

In recent decades, there has been great interest in gradient metasurfaces, which are nonperiodic surfaces aimed at wave-front manipulation for beam-steering applications in near or far fields [39]. Such surfaces can be designed with use of the ray-optics approach [40], the equivalence principle (Huygens metasurfaces) [41], the geometric phase approach [42] or programmable-design generation [43]. Here we present an alternative approach to design such surfaces by engineering EFCs. We show that we are able to steer the surface wave to propagate smoothly along specified curved paths using an inhomogeneous metasurface made of rotated C-shaped unit cells. The inhomogeneous

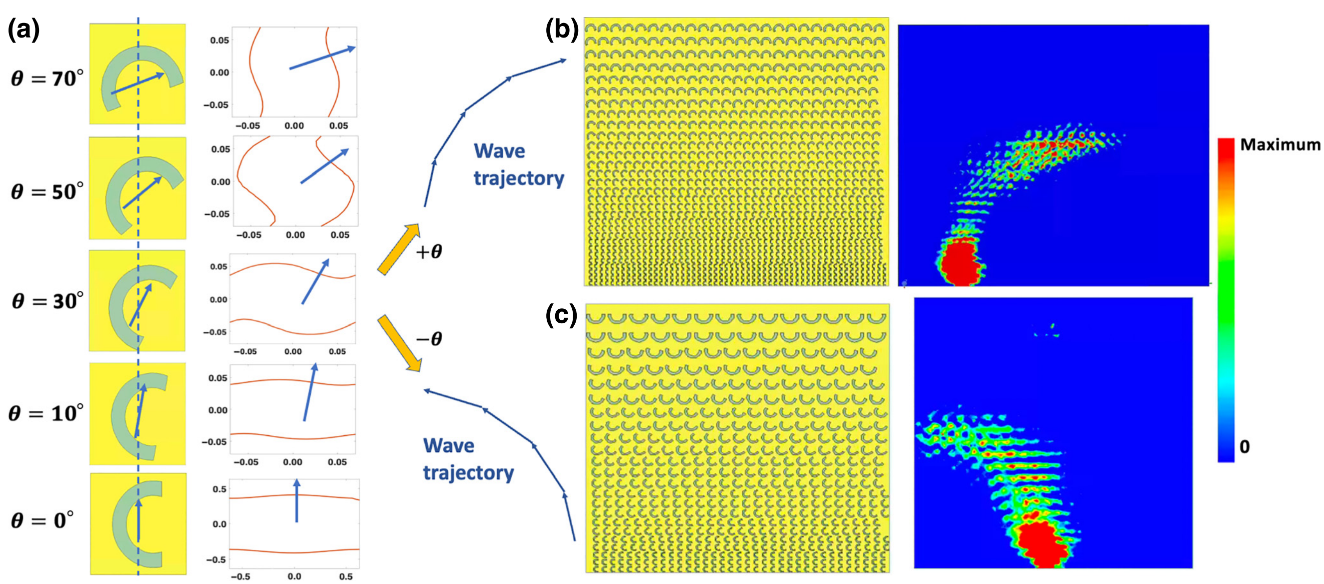

FIG. 4. (a) Rotated C-shaped unit cells at a rotation angle θ ranging from 0° to 70° and their corresponding EFCs. The two wave trajectories formed when θ is positive and when θ is negative are demonstrated. The designed inhomogeneous C-shaped metasurfaces and their calculated electric field profiles are shown to steer the surface wave along curved paths towards (b) the right and (c) the left at 19 GHz.

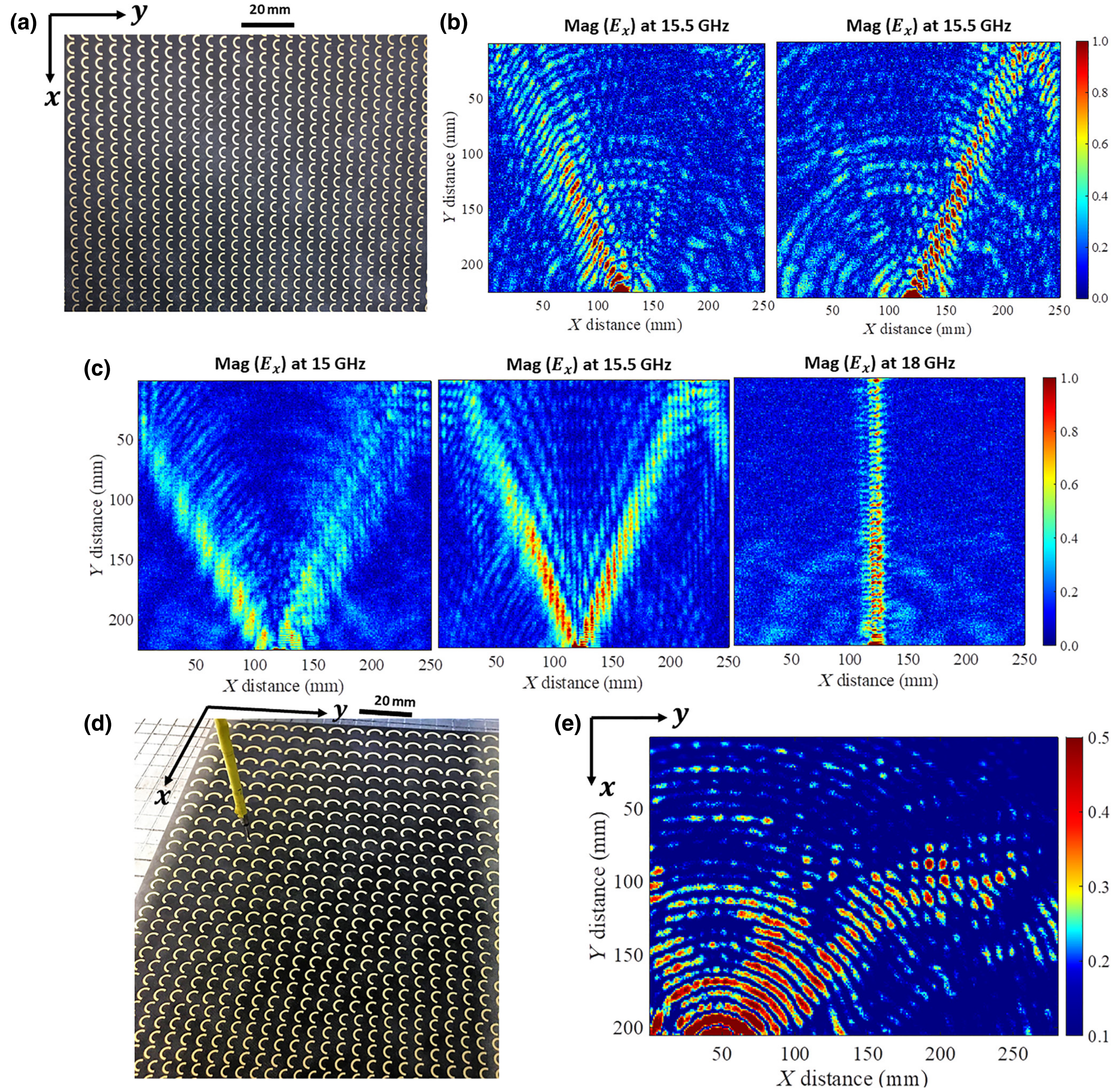

FIG. 5. (a) Photograph of the fabricated C-shaped metasurface. (c) Measured E_x maps at frequencies of 15 to 18 GHz showing the different wave split angles for excitation with E_y, where the highly collimated wave propagation is shown at 18 GHz. (b) Measured E_x for the C-shaped metasurface at 15.5 GHz when it is excited with $E_y + iE_z$ (left) and $E_y - iE_z$ (right) at the bottom center, showing the spin-dependent propagation behavior. (d) Photograph of the fabricated inhomogeneous C-shaped metasurface. (e) Measured E_z profile at 18.5 GHz showing the surface-wave propagation along a curved path.

design is simply done by our mapping the rotated C-shaped unit cells and their angle of collimation using the EFCs to form the specified wave path.

A. Rotation angle and EFC

Figure 4(a) shows the design steps to make the inhomogeneous metasurface designs shown in Figs. 4(b) and 4(c) through engineering the EFC. With a focus on the C shapes highly collimated EFC, it can be shown that rotating the C-shaped unit cell results in rotating its EFC by almost the same angle of rotation, θ. For simplicity, we show schematics for five rotated unit cells at $\theta = 0^\circ$ to $\theta = 70^\circ$ and their corresponding EFCs. The blue arrows indicate the propagation direction of the wave. The wave trajectory deduced from the EFCs of the rotated C-shaped unit cells when positive θ values are used is shown at the top right in Fig. 4(a), while the wave trajectory when negative θ values are used, where the wave is steered to the left, is shown at the bottom right in Fig. 4(a).

Figures 4(b) and 4(c) show the inhomogeneous metasurface designs for the two wave paths described earlier. The design shown in Fig. 4(b) is composed of 30 columns divided into nine groups. In each group, θ is increased by 10° and the shape is scaled up by a scaling factor, s. This is because rotating the unit cell results in a slight increase in its supported surface-wave frequency. To eliminate the frequency mismatch, each rotated C-shaped unit cell is scaled up by a scaling factor of 1.11. This scaling factor is deduced from our mapping the rotation angles and the resulting frequency shift. More information on how the scaling factor was deduced from our calculating the frequency shift for each rotation angle can be found in Supplemental Material [34]. The scaling factor, s, of a unit cell can be defined in terms of its rotation angle as follows:

$$s = 1.11^{\frac{\theta}{10}}. \tag{2}$$

B. Surface-wave steering

The electric field profiles for the two inhomogeneous metasurface designs at 19 GHz are presented on the right in Figs. 4(b) and 4(c), showing the smooth steering of the surface wave along curved paths. The demonstrated steered wave is spin independent since we worked with the highly collimated, spin-independent contour. This means that the same electric field profile can be achieved with a linearly or circularly polarized excitation source. This demonstrates how EFC engineering for wave steering provides the capability of smoothly steering the surface wave along predetermined paths without much complexity in the design process, where the same unit-cell design is used. More discussion on the observed electric field enhancement at the higher bending angles can be found in Supplemental Material [34].

IV. EXPERIMENTAL RESULTS

The C-shaped metasurface was fabricated and measured. Figure 5(a) shows a photograph of the fabricated homogeneous (periodic) C-shaped metasurface, while the inhomogeneous (graded) surface is shown in Fig. 5(d). These photographs ate not to scale with the electric field plots. Scale bars are shown at the top of the metasurfaces photographs for clarification. The C-shaped structures are made of copper, and are placed on top of a Roger's 5880 substrate of thickness 0.381 mm. An E_y probe is used to excite the surface, which is placed at the bottom center. An E_x measuring probe is attached to a moving station, which is programmed to scan the surface point by point. Both probes are connected to a vector network analyzer, where the magnitude and phase of the transmitted wave (S21) are measured. Hence, the magnitude and phase of E_x can be extracted for the whole surface at different frequencies, showing the different wave-propagation properties as shown in Fig. 5(b), which matches the simulation results shown in Fig. 2(b). The electric field profile shown in Fig. 5(c) is measured for the homogeneous C-shaped surface at 15.5 GHz when it is excited with a circularly polarized dipole source. The circularly polarized dipole excitation is done through excitation with E_y and E_z dipole sources separately. E_y and E_z excitations are achieved with two probe antennae oriented along the y direction and the z direction, respectively. The magnitude and phase of E_x are measured for each excitation separately and are then added with a 90° phase shift with use of the following equation:

$$\mathbf{E}_x^y \pm i\mathbf{E}_x^z = |\mathbf{E}_x^y| \cos\left(\phi_x^y\right) + |\mathbf{E}_x^z| \cos\left(\phi_x^z \pm 90^\circ\right), \tag{3}$$

where $\mathbf{E}_x^y$ ($\mathbf{E}_x^z$) is the measured $\mathbf{E}_x$ for excitation with a probe along the y (z) axis. The E_z profile is measured for the inhomogeneous metasurface at 18.5 GHz and is shown in Fig. 5(d), which demonstrates the surface-wave steering along the predefined path. Some mismatch between the experimental and simulation results can be observed due to the imperfection of the probe excitation resulting in the excitation of unwanted modes in addition to probe placement close to the edge of the surface, which can lead to some reflections around the corner of the metasurface.

V. CONCLUSION

In this paper we studied numerically and experimentally a metallic C-shaped metasurface and its various wave-propagation and wave-polarization properties. We showed that due to the broken rotational symmetry of the C-shaped design, it possesses high self-collimation. Additionally, we studied the spin-momentum-locking phenomenon in the C-shaped design by calculating its spin density and showed it is capable of spin-dependent wave splitting, where the split angle can be changed by tuning of the frequency. We also showed two inhomogeneous metasurface designs to steer the wave along defined curved paths by rotating the C-shaped design's EFCs and scaling their sizes to eliminate frequency mismatch. This work emphasizes that engineering EFCs can be used as a powerful and simple design tool to achieve a wide range of wave properties: spin-dependent wave splitting, highly confined waveguiding, and wave steering along defined paths.

ACKNOWLEDGMENTS

This work was supported by the AFOSR under Grant No. FA9550-21-1-0167 and the ONR under Grant No. N00014-20-1-2710.

[1] N. Yu and F. Capasso, Flat optics with designer metasurfaces, Nat. Mater. **13**, 139 (2014).
[2] W. T. Chen, A. Y. Zhu, and F. Capasso, Flat optics with dispersion-engineered metasurfaces, Nat. Rev. Mater. **5**, 604 (2020).
[3] N. Yu, P. Genevet, F. Aieta, M. A. Kats, R. Blanchard, G. Aoust, J.-P. Tetienne, Z. Gaburro, and F. Capasso, Flat optics: Controlling wavefronts with optical antenna metasurfaces, IEEE J. Sel. Top. Quantum Electron. **19**, 4700423 (2013).
[4] F. Capasso, The future and promise of flat optics: A personal perspective, Nanophotonics **7**, 953 (2018).
[5] H.-T. Chen, A. J. Taylor, and N. Yu, A review of metasurfaces: Physics and applications, Rep. Prog. Phys. **79**, 076401 (2016).
[6] A. Li, S. Singh, and D. Sievenpiper, Metasurfaces and their applications, Nanophotonics **7**, 989 (2018).
[7] R. Quarfoth and D. Sievenpiper, Artificial tensor impedance surface waveguides, IEEE Trans. Antennas Propag. **61**, 3597 (2013).
[8] J. B. Dia'aaldin and D. F. Sievenpiper, Guiding waves along an infinitesimal line between impedance surfaces, Phys. Rev. Lett. **119**, 106802 (2017).
[9] J. Lee and D. F. Sievenpiper, Patterning technique for generating arbitrary anisotropic impedance surfaces, IEEE Trans. Antennas Propag. **64**, 4725 (2016).
[10] S. A. Kuznetsov, M. A. Astafev, M. Beruete, and M. Navarro-Cía, Planar holographic metasurfaces for terahertz focusing, Sci. Rep. **5**, 1 (2015).
[11] F. Ding, Y. Chen, and S. I. Bozhevolnyi, Focused vortex-beam generation using gap-surface plasmon metasurfaces, Nanophotonics **9**, 371 (2020).
[12] F. Ding, Y. Chen, and S. I. Bozhevolnyi, Gap-surface plasmon metasurfaces for linear-polarization conversion, focusing, and beam splitting, Photonics Res. **8**, 707 (2020).
[13] X. Chen, H. Zou, M. Su, L. Tang, C. Wang, S. Chen, C. Su, and Y. Li, All-dielectric metasurface-based beam splitter with arbitrary splitting ratio, Nanomaterials **11**, 1137 (2021).
[14] Y. Yang, L. Jing, L. Shen, Z. Wang, B. Zheng, H. Wang, E. Li, N.-H. Shen, T. Koschny, C. M. Soukoulis, and Hongsheng Chen, Hyperbolic spoof plasmonic metasurfaces, NPG Asia Materials **9**, e428 (2017).
[15] D. F. Sievenpiper, Forward and backward leaky wave radiation with large effective aperture from an electronically tunable textured surface, IEEE Trans. Antennas Propag. **53**, 236 (2005).
[16] W. Liu, H. Cheng, J. Tian, and S. Chen, Diffractive metalens: From fundamentals, practical applications to current trends, Adv. Phys.: X **5**, 1742584 (2020).
[17] D. W. Prather, S. Shi, J. Murakowski, G. J. Schneider, A. Sharkawy, C. Chen, B. Miao, and R. Martin, Self-collimation in photonic crystal structures: A new paradigm for applications and device development, J. Phys. D: Appl. Phys. **40**, 2635 (2007).
[18] Y.-C. Chuang, 2010, Ph.D. thesis, (The University of North Carolina at Charlotte).
[19] J. Witzens, M. Loncar, and A. Scherer, Self-collimation in planar photonic crystals, IEEE J. Sel. Top. Quantum Electron. **8**, 1246 (2002).
[20] K. Y. Bliokh and F. Nori, Transverse spin of a surface polariton, Phys. Rev. A **85**, 061801 (2012).
[21] K. Y. Bliokh, A. Y. Bekshaev, and F. Nori, Extraordinary momentum and spin in evanescent waves, Nat. Commun. **5**, 1 (2014).
[22] K. Y. Bliokh, D. Smirnova, and F. Nori, Quantum spin Hall effect of light, Science **348**, 1448 (2015).
[23] J. Hirsch, Spin Hall effect, Phys. Rev. Lett. **83**, 1834 (1999).
[24] D. O'connor, P. Ginzburg, F. J. Rodríguez-Fortuño, G. A. Wurtz, and A. V. Zayats, Spin–orbit coupling in surface plasmon scattering by nanostructures, Nat. Commun. **5**, 1 (2014).
[25] S. M. Kandil and D. F. Sievenpiper, C-shaped chiral waveguide for spin-dependent unidirectional propagation, Appl. Phys. Lett. **118**, 101104 (2021).
[26] J. Lin, J. B. Mueller, Q. Wang, G. Yuan, N. Antoniou, X.-C. Yuan, and F. Capasso, Polarization-controlled tunable directional coupling of surface plasmon polaritons, Science **340**, 331 (2013).
[27] D. J. Bisharat and D. F. Sievenpiper, Electromagnetic-dual metasurfaces for topological states along a 1D interface, Laser Photonics Rev. **13**, 1900126 (2019).
[28] W.-S. Ruan, X.-T. He, F.-L. Zhao, and J.-W. Dong, Analysis of unidirectional coupling in topological valley photonic crystal waveguides, J. Lightwave Technol. **39**, 889 (2020).
[29] L. Huang, X. Chen, B. Bai, Q. Tan, G. Jin, T. Zentgraf, and S. Zhang, Helicity dependent directional surface plasmon polariton excitation using a metasurface with interfacial phase discontinuity, Light: Sci. Appl. **2**, e70 (2013).
[30] M. F. Picardi, A. Manjavacas, A. V. Zayats, and F. J. Rodríguez-Fortuño, Unidirectional evanescent-wave coupling from circularly polarized electric and magnetic dipoles: An angular spectrum approach, Phys. Rev. B **95**, 245416 (2017).
[31] M. F. Picardi, A. V. Zayats, and F. J. Rodríguez-Fortuño, Janus and Huygens dipoles: Near-field directionality beyond spin-momentum locking, Phys. Rev. Lett. **120**, 117402 (2018).
[32] F. J. Rodríguez-Fortuño, G. Marino, P. Ginzburg, D. O'Connor, A. Martínez, G. A. Wurtz, and A. V. Zayats, Near-field interference for the unidirectional excitation of electromagnetic guided modes, Science **340**, 328 (2013).
[33] I. H. Giden, M. Turduev, and H. Kurt, Broadband super-collimation with low-symmetric photonic crystal, Photonics Nanostructures-Fundam. Appl. **11**, 132 (2013).
[34] See Supplemental Material at http://link.aps.org/supplemental/10.1103/PhysRevApplied.21.044006 for additional information on the electric field propagation plots and calculations of the frequency shift resulting from rotation of the C-shaped unit cells.
[35] Y. Yermakov, A. I. Ovcharenko, A. A. Bogdanov, I. V. Iorsh, K. Y. Bliokh, and Y. S. Kivshar, Spin control of light with hyperbolic metasurfaces, Phys. Rev. B **94**, 075446 (2016).
[36] D. Gao, Z. Zhou, and D. S. Citrin, Self-collimated waveguide bends and partial bandgap reflection of photonic crystals with parallelogram lattice, JOSA A **25**, 791 (2008).
[37] Y. Xu, X.-J. Chen, S. Lan, Q. Guo, W. Hu, and L.-J. Wu, The all-angle self-collimating phenomenon in photonic crystals with rectangular symmetry, J. Opt. A: Pure Appl. Opt. **10**, 085201 (2008).

[38] S. M. Kandil, D. J. Bisharat, and D. F. Sievenpiper, Chiral surface wave propagation with anomalous spin-momentum locking. *ACS Photonics*.
[39] N. M. Estakhri and A. Alù, Recent progress in gradient metasurfaces, JOSA B **33**, A21 (2016).
[40] N. Yu, P. Genevet, M. A. Kats, F. Aieta, J.-P. Tetienne, F. Capasso, and Z. Gaburro, Light propagation with phase discontinuities: generalized laws of reflection and refraction, science **334**, 333 (2011).
[41] C. Pfeiffer and A. Grbic, Metamaterial Huygens' surfaces: Tailoring wave fronts with reflectionless sheets, Phys. Rev. Lett. **110**, 197401 (2013).
[42] M. V. Berry, The adiabatic phase and Pancharatnam's phase for polarized light, J. Mod. Opt. **34**, 1401 (1987).
[43] H. Yang, X. Cao, F. Yang, J. Gao, S. Xu, M. Li, X. Chen, Y. Zhao, Y. Zheng, and S. Li, A programmable metasurface with dynamic polarization, scattering and focusing control, Sci. Rep. **6**, 1 (2016).